A mathematical method for extracting cell secretion rate from affinity biosensors continuously monitoring cell activity

Yandong Gao,[a] Qing Zhou, Zimple Matharu, Ying Liu, Timothy Kwa, and Alexander Revzin[a]
Department of Biomedical Engineering, University of California, Davis, California 95616, USA

(Received 10 March 2014; accepted 21 April 2014; published online 30 April 2014)

Our laboratory has previously developed miniature aptasensors that may be integrated at the site of a small group of cells for continuous detection of cell secreted molecules such as inflammatory cytokine interferon gamma (IFN-γ). In a system such as this, the signal measured at the sensor surfaces is a complex function of transport, reaction, as well as of cellular activity. Herein, we report on the development of a mathematical framework for extracting cell production rates from binding curves generated with affinity biosensors. This framework consisted of a diffusion-reaction model coupled to a root finding algorithm for determining cell production rates values causing convergence of a predetermined criterion. To experimentally validate model predictions, we deployed a microfluidic device with an integrated biosensor for measuring the IFN-γ release from CD4 T cells. We found close agreement between secretion rate observed theoretically and those observed experimentally. After taking into account the differences in sensor geometry and reaction kinetics, the method for cell secretion rate determination described in this paper may be broadly applied to any biosensor continuously measuring cellular activity. © *2014 AIP Publishing LLC*.
[http://dx.doi.org/10.1063/1.4874216]

I. INTRODUCTION

There has been significant interest in developing biosensors that produce signals in reagent-less and label-less manner. In addition to surface plasmon resonance (SPR), quartz crystal microbalance (QCM), and other sensing techniques that do not use labels altogether,[1–3] there are a number of beacon technologies that employ labels to transduce biological event into an optical or electrical signal.[4] These beacons emit signal directly upon the binding of target analyte without the need for additional reagents or labels. Aptamer beacons are one category of reagent-less beacons.[5,6] A particularly promising direction is to employ aptamers in place of antibodies for affinity sensing strategies that report on the presence of analytes such as proteins.[7–13] In contrast to antibody-based immunoassays, aptamer-based affinity assays detect presence of target proteins directly, without the need for multiple washing and labeling steps and also provide dynamic information about protein binding.[14,15]

The amount and the type of molecules secreted into the extracellular space may be used to infer about cell phenotype, differentiation, and response to injury. Immunology, in particular, is heavily reliant on monitoring cellular secretion of proteins to determine cell functions (e.g., T helper or macrophage types).[16–18] In light of this, there has been an increased interest in developing biosensors for local and dynamic detection of cell secreted factors. The examples include the development of microenvgraving system for detecting cytokine release from single immune

[a]Authors to whom correspondence should be addressed. Electronic addresses: ydgao@ucdavis.edu and arevzin@ucdavis.edu.

cells[19–21] and the use of microresonators for continuous monitoring of cytokine release by T cells.[22–24] Given the dearth of approaches for determining dynamics of cell secretions, the biosensing technologies hold considerable promise for determining when cell secretion commences and how it changes over time. Several groups have reported to dynamically monitor cellular release of molecules by a continuous-flow microfluidic system.[25–31] Sample was collected from cultured cells and analyzed with an on-line enzyme assay. Without complicated microfluidic design and connections, our laboratory has described microsystems integrating aptamers with microfluidics for continuous monitoring of inflammatory cytokines released by small groups of cells.[32–34] However, determining changes in cell secretion rate over time has remained a challenge. The complexity lies in the fact that the signal recorded by the affinity biosensor is a function of multiple factors, including cell secretion rate, protein concentration, transport, and surface reaction. Fig. 1(a) shows pictorially the factors that need to be considered in order to determine cell secretion rate.

In this paper, we describe a mathematical method for deriving secretion rates from aptasensor binding curves. This method couples diffusion-reaction modeling with root finding algorithm for determining secretion for defined time increments. To validate this mathematical framework, we used aptasensors for detection of inflammatory cytokine interferon gamma (IFN-γ)—a technology that is well established in our lab.[12] Sensing electrodes were integrated with reconfigurable microsystem shown in Figs. 1(b) and 1(c) to allow breaking up cell secretion experiments into precise time increments through a series of detect-and-regenerate steps. The secretion rates determined experimentally in reconfigurable microfluidic devices were consistent with rates determined mathematically, validating utility of our approach.

II. MATERIALS AND METHODS

A. Chemicals and materials

1× phosphate-buffered saline (PBS) without calcium and magnesium, Na_4EDTA, $KHCO_3$, NH4Cl, anhydrous toluene, 11-Mercaptoundecanoic acid (MUA), 200-proof ethanol, urea, 4-(2-Hydroxyethyl)-1-piperazineethanesulfonic acid (HEPES), sodium bicarbonate ($NaHCO_3$), 6-mercapto-1-hexanol (MCH), and tris(2-carboxyethyl)phosphine hydrochloride (TCEP) were purchased from Sigma-Aldrich (St. Louis, MO). Chromium etchant (CR-4S) and gold etchant (Au-5) were purchased from Cyanteck Corporation (Fremont, CA). Positive photoresist (S1813) and developer solution (MIF-318) were purchased from Dow Chemical (Marlborought, MA).

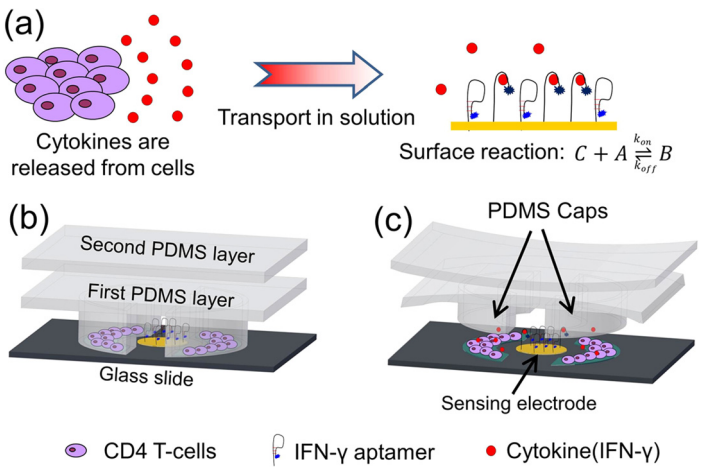

FIG. 1. (a) Cell secretion signals measured using aptamer-modified electrodes are a function of diffusion and surface binding of the detected molecules. We developed an algorithm for determining up and down changes in cell secretion rates based on the binding curves. (b) and (c) Reconfigurable microfluidic device used to test validity of the mathematical algorithm. The device was used to measure secretion of IFN-γ, and then regenerate the sensor, then measure IFN-γ again. Using this approach, we experimentally determined secretion rates at different time intervals during a cell secretion experiment.

Negative photoresist (SU8-2050 and SU8-2010) and developer solution (SU8-developer) were purchased from MicroChem (Newton, MA). Polydimethylsiloxane (PDMS, Sylgard 184) was purchased from Dow Corning (Midland, MI). Tygon microbore tube was obtained from Cole-Parmer (Vermon Hills, IL). Pyrex Cloning cylinders (8 mm × 8 mm) were purchased from Fisher Scientific (Pittsburgh, PA). 3-Acryloxypropyl trichlorosilane was purchased from Gelest, Inc. (Morrisville, PA). Polyethylene Glycol Diacrylate (PEG-DA, MW = 6000) was purchased from SunBio Co. Ltd (Ansan, Korea), and photoinitiator (Irgacure 2959) was purchased from Ciba (Switzerland). The film masks for electrodes and microfluidic channels were designed in AutoCAD and printed by CAD/Art Services (Bandon, OR). Human recombinant IFN-γ was from R&D Systems (Minneapolis, MN). Monoclonal purified mouse anti human CD4 Abs were obtained from Beckman-Coulter (Fullerton, CA). Cell culture medium RPMI 1640 with L-glutamine was purchased from VWR (West Chester, PA). Medium was supplemented with fetal bovine serum (FBS) and penicillin/streptomycin purchased from Life Technologies (Grand Island, NY). T cells activation reagents, phorbol 12-myristate 13-acetate (PMA) and ionomycin were purchased from Sigma-Aldrich. Methylene blue (MB), carboxylic acid, and succinimidyl ester were received from MB-NHS, Biosearch Technologies, Inc. (Novato, CA). The 34-mer IFN-γ-binding aptamer sequence was obtained from IDT Technologies (San Diego, CA).

B. Preparation of MB-tagged aptamer

The MB-tagged aptamer was prepared using a procedure similar to that described previously.[12,33] Briefly, NHS-labeled MB was conjugated to the 5′-terminal of an amino-modified DNA aptamer through succinimide ester coupling. After reaction, the sample was filtered using a centrifugal filter. The stock aptamer solution (50 μM) was stored at −20 °C for future use.

C. SPR analysis

SPR experiments were performed using BI-3000 SPR system (Biosensing Instrument, Inc., Tempe, AZ) and BI untreated gold sensor chips. 1 μM MB-tagged aptamer was diluted in HEPES buffer and incubated on the sensor chip overnight at 4 °C. The sensor chip was washed with HEPES buffer three times and then incubated with 3 mM MCH for 1 h at room temperature. After rinsing with HEPES buffer, the sensor chip was mounted on the SPR system as the instruction manual. Recombinant IFN-γ solutions ranging from 0.1 μg/ml to 5 μg/ml were prepared in HEPES buffer and injected in the analyte channel with a contact time of 240 s, dissociation time of 360 s, and a flow rate of 30 μl/min. All experiments were conducted at 25 °C and repeated in triplicate. The sensorgrams were fitted globally using the BI kinetics analysis program. The association rate (k_{on}), dissociation rate (k_{off}), and binding constant (K_d) were derived from the fitted curves.

D. Fabrication of micropatterned electrodes

The electrodes were fabricated using standard photolithography and metal-etching process. Glass slides coated with 15 nm Cr adhesion layer and 100 nm Au layer were purchased from Lance Golddard Association. A protection photoresist layer was spin coated at the speed of 2000 rpm. After baking for 1 min at 115 °C, the pattern was exposed under UV through a plastic photomask and then developed in MF-319 buffer. Subsequently, the slides were immersed in Au and Cr etching buffer to create the electrodes. Each Au electrode was 300 μm in diameter and was connected to a 2 mm × 2 mm square contact pad via a 20 μm wide lead. The substrates were sonicated in acetone, followed by de-ionized (DI) water, to remove the photoresist and then dried by nitrogen for future use.

E. Fabrication of microfluidic device

The microfluidic platforms were fabricated by standard soft lithography techniques using replica molding.[35,36] Two layers of PDMS were used to form the valve-enabled device as described previously.[37,38] After the solidified PDMS were peeled from their molds, a sharp

metal puncher was first used to generate holes for the microbore tubes in the second PDMS layer. The first and the second PDMS layers were then bonded together after treatment by oxygen plasma. A strong irreversible bonding was formed in this way to sustain a high pressure in the control chamber. Holes for inlets and outlets were then punched through both layers. The PDMS piece was finally bonded to substrate with electrodes using negative pressure to form the functional device.[39]

F. Immobilization of aptamer on gold electrodes

Prior to immobilization, aptamer stock solution was reduced in 10 mM TCEP for 1 h to cleave disulfide bonds. The MB-tagged aptamer was diluted in HEPES buffer to 1 μM and then flow into the microfluidic channels. The whole device was placed in 4 °C refrigerator overnight for immobilization. The microfluidic channel was washed with HEPES buffer three times and then incubated with 3 mM MCH for 1 h at room temperature. After rinsing with HEPES buffer, the microfluidic device was ready for electrochemical experiments.

G. Electrochemical detection

Electrochemical measurements were carried out using a CHI 842B potentiostat (CH Instruments, Austin, TX) as described previously.[33] The electrochemical cell consisted of a flow-through Ag/AgCl reference electrode inserted at the outlet, a Pt wire counter electrode placed in the inlet of the microfluidic device, and Au working electrode inside the microfluidic channel. The electrode arrays were connected to the potentiostat via the contact pads. Square Wave Voltammetry (SWV) scans were performed at a frequency of 60 Hz over the range from −0.1 to −0.50 V. The potentiostat was connected to the computer via ER-16 electromechanical relay (National Instruments, TX). A program was written in Sikuli to interface the NI software and CHI software which allows for controlled switching between different pair of working/reference electrodes and taking measurements at defined time intervals.

H. Capture of CD4 T cells and detection of IFN-γ release

After immobilizing MB-labeled IFN-γ aptamer onto gold, anti-CD4 Ab (0.1 mg/ml) was first flowed in the channel to coat on the surface for 1 h. Human lymphocytes were prepared as described previously.[33] The cells were introduced into the channel at a flow rate of 5 μl/min. After CD4 T cells were captured, the protection microcups were lowered to protect cells by increasing the pressure into the control chamber. Subsequently, 7M urea buffer was loaded into the channel to remove cells remaining outside of the microcups. After rinsing with low-serum RPMI media, the microcups were lifted up by releasing the pressure in the control chamber. As a result, a small population of CD4 T cells was confined next to an electrode. The microfluidic channel was then filled with mitogenic agent to activate cells for electrochemical production. The mitogenic solution consisted of PMA and ionomycin dissolved to concentration of 50 ng/ml and 1 μg/ml, respectively, in low-serum RPMI 1640 media.

This microsystem was operated in either continuous or discontinuous (phased) mode. In continuous mode, microcups were permanently raised and the electrode was exposed to cell-secreted cytokine molecules for the duration of experiment (Figs. 2(a) and 2(c)). In this mode, SWV measurements were taken every 10 min for up to 2.5 h post stimulation. In phased mode, the sensing electrodes were exposed to cell-secreted cytokines for 30 min after which the microcups were lowered to protect the cells and the electrodes were regenerated by flushing the channel with 7M urea buffer (Fig. 2(d)). We have previously developed this device in order to enable selective exposure of the aptasensor to denaturation buffers (e.g. 7M urea) without harming the neighboring cells, regenerating the sensor and extending the duration of cell sensing experience.[34] After rinsing the chamber with low-serum RPMI media, the cell protection cups were raised again to restart IFN-γ monitoring. The process of IFN-γ signal collection followed by electrode regeneration was repeated four times. We chose to utilize this device in the present paper because it allows to break a cell secretion monitoring experiment into several time

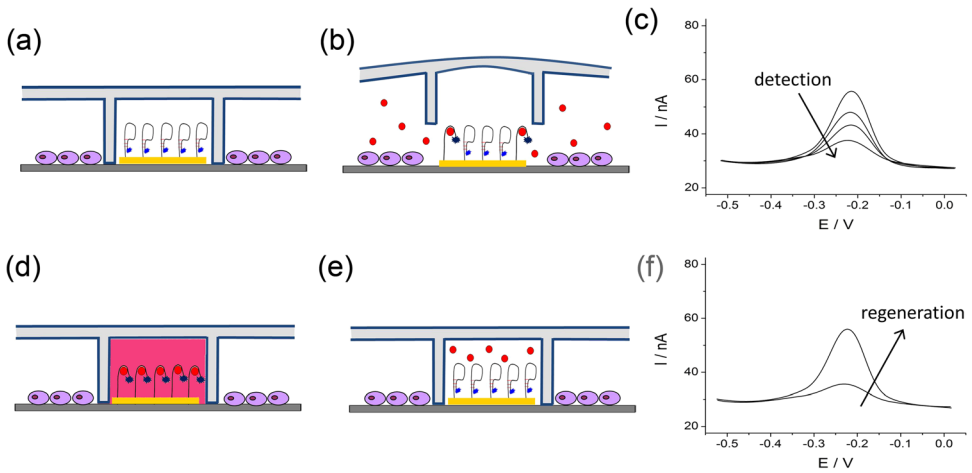

FIG. 2. Working principle of the microfluidic device. (a) Cells are seeded inside the PDMS cups. (b) PDMS cups are lifted for detection. (c) A schematic of SWV signals during detection. Redox current goes down as more secreted molecules bind to the electrode. (d) To regenerate a sensor after a predertimned time of signal collection, PDMS cups are pressed down to protect the cells and regeneration buffer is introduced. (e) The aptasensor is ready for another round of measurement. (f) The redox activity of the electrode is recovered after regeneration process with SWV signal returning to original, pre-detection level.

segments and to determine secretion rate for each segment. Thus, the device mimics experimentally the theoretical algorithm being developed in this paper.

I. Numerical simulations

COMSOL Multiphysics 4.3a and Livelink® for Matlab (COMSOL, Inc., Los Angeles, CA) were used to solve the partial differential equations relating diffusion and surface binding. A Matlab script was written to set up the COMSOL model and utilize the root-finding algorithm. In constructing the model, we use the geometry and sensor configuration of the actual sensing devices used for experimental verification. The main model parameters are listed in Table I.

III. MATHEMATICAL MODEL

A. Reaction-diffusion model

We first developed a numerical model that accounts for the secretion of cytokine from cells, the transport of those cytokines in the microfluidic channel, and the binding of those cytokines to the aptamers immobilized on the electrode surface. Since the microfluidic channel is sealed during the experiment, the convection was assumed to be negligible. Diffusion-based transport was governed by the following equation:

$$\frac{\partial C}{\partial t} = D\nabla^2 C, \tag{1}$$

where C is the concentration of cytokine in the media and D is the diffusion coefficient of the cytokine. The binding of secreted cytokine molecules to the aptamer layer was modeled by the first-order Langmuir kinetics,[42,43]

TABLE I. Main parameters used in simulations.

Diffusion coefficient (D)	1.475×10^5 cm^2/s (Ref. 40)
Surface binding density (A_0)	2.2×10^{12} mol/cm^2 (Ref. 41)
Association rate constant (k_{on})	1.38×10^5 1/s·M
Dissociation rate constant (k_{off})	6.339×10^{-5} 1/s

$$\frac{dB}{dt} = k_{on}C(A_0 - B) - k_{off}B, \tag{2}$$

where B is cytokine-aptamer complex on the sensor surface; A_0 is the initial surface concentration of aptamer; and k_{on} and k_{off} is the association and disassociation constant, respectively. The surface reaction and bulk diffusion are coupled together through the boundary condition on the sensor surface

$$-D\frac{\partial \text{C}}{\partial n} = -k_{on}C(A_0 - B) + k_{off}B, \tag{3}$$

where $-D\frac{\partial \text{C}}{\partial n}$ is the molar flux of C normal to the sensor surface (n is the outward normal).

In the cell detection process, we assume that the initial cytokine concentration in solution and on the sensor surface after stimulation is zero. Therefore, the initial condition is $C = 0$ and $B = 0$ at $t = 0$. There is an additional boundary condition accounting for cytokine secretion from cells,

$$-D\frac{\partial \text{C}}{\partial n} = \dot{\sigma}\frac{N_c}{A_c}, \tag{4}$$

where $\dot{\sigma}$ is the cell secretion rate and N_{c} is the total number of cells captured in the antibody coated region A_{c}. The measured signal S(t) is the integration of the ratio of bound molecules to total available binding cites over the whole sensor surface Ω (Ref. 44),

$$S(\text{t}) = \int \frac{B(t)}{A_0} d\Omega. \tag{5}$$

B. Root-finding algorithm

The mathematical model described above is set up in COMSOL Multiphysics. The geometry and parameters, such as D, k_{on}, k_{off}, A_0, and $\dot{\sigma}$, are all known and are input into the model. The simulation software (COMSOL) solves these equations and calculates the concentration field (C) in the fluidic domain and cytokine-aptamer complex (B) on the sensor surface. The resulting signal obtained according to Eq. (5) becomes a complex function depending on the model parameters,

$$S = \mathcal{F}(D, k_{on}, k_{off}, A_0, \dot{\sigma}, \ldots). \tag{6}$$

The secretion rate $\dot{\sigma}$ is one of model parameters and its value is unknown. In order to determine the value of $\dot{\sigma}$ for which Eq. (6) is satisfied, we set up a root-finding algorithm to solve this equation numerically.

Our strategy for finding the root for Eq. (6) is shown in Fig. 3(a). Starting from a known concentration field at t_1 which was either the initial condition or the result from last simulation, a trial secretion rate was estimated to be constant during the time interval from t_1 to t_2. After inputting these parameters in COMSOL, the diffusion equation was solved and concentration field (C) and surface binding (B) at time t_2 were determined. The simulated signal was calculated according to Eq. (5). We then compared the calculated signal with the measured signal at time t_2. If these two signals were close enough to fall within a predetermined criterion, the estimated secretion rate was accepted; otherwise a new estimation was generated and the whole procedure was repeated until an acceptable secretion rate was obtained. The convergence criterion is that $\|\text{S} - S_{exp}\| < \epsilon S_{exp}$, where S_{exp} is the signal from experiment and ϵ was chosen as 10^{-4} in this paper.

The critical question was how to generate a new estimated value based on previous information? Because the functional form and the derivative of $\mathcal{F}$ in Eq. (6) are unknown, a

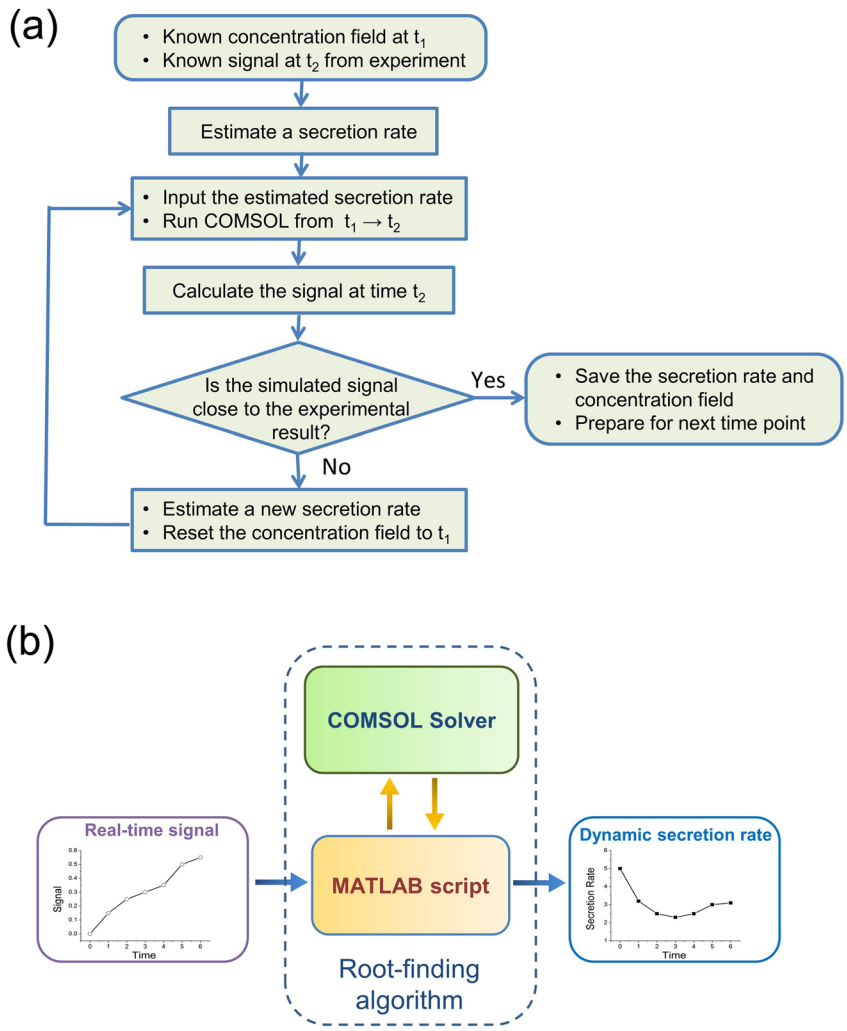

FIG. 3. (a) Strategy of simulations and (b) main structure of the program.

numerical root-finding approach, Brent's method,[45] was used to find the value of $\dot{\sigma}$. It combines root bracketing, bisection, and inverse quadratic interpolation and converges quickly. However, Brent's algorithm requires a sign change over an interval which means that two trial rates are found. One rate results in the value of S that is larger while the other rate produces S value that is smaller than the experimental value S_{exp}. The solution is "bracketed" in this interval between the two secretion rate values. To resolve this, we also included the secant method.[46] If there is no sign change over the initial guessed interval, secant method runs until convergence or finding a sign change. If a bracket is found, Brent's method will take over to find the root inside the bracket.

In this model, the previous secretion rate was used as the starting point to determine the secretion rate over next time interval. For the first time point, we used 0.0079 pg/h/cell a value that was determined by us previously using constant rate assumption.[33]

Livelink for MATLAB integrates COMSOL Multiphysics with MATLAB to extend user's modeling ability. We wrote a MATLAB script to utilize the modified Brent's method. The script was used to set up a COMSOL model, manipulate the program flow, and analyze results in the MATLAB scripting environment. This modular programming technique allows us to separate the functionality of the program into two independent modules (Fig. 3(b)), which makes it convenient to improve our method in future development. For example, other root-finding algorithm can easily replace the Brent's method used in this work. Taking advantage of COMSOL

Multiphysics, more complicated models such as those including convection or activator/inhibitor in reaction can be implemented in the future studies.

IV. RESULTS AND DISCUSSION

The goal of this study was to develop a mathematical method to convert dynamic signal from reagent-less affinity biosensor into dynamic cell secretion rate. The resultant method allows quantifying up and down changes in cell secretion from the shape of the binding curve measured by the affinity biosensor placed next to the cells.

A. Kinetics parameters

The IFN-γ cytokine-aptamer interactions were first characterized by SPR to determine reaction constants that could later be used for constructing reaction-diffusion model. Thiolated aptamers were immobilized on SPR sensing chips and then challenged with varying concentrations of IFN-γ. Each sensing chip corresponded to one concentration. Fig. 4 shows average of three responses to each concentration. Those curves were fitted by first-order reaction model using the BI kinetics analysis program (Scrubber). The association rate, k_{on}, was determined to be 1.38×10^5 1/s·M and disassociation rate, k_{off}, was 6.339×10^{-5} 1/s. The equilibrium constant, $K_d = 0.46$ nM, is similar to the value of 0.34 nM we reported previously.[12]

B. Testing algorithm validity with simulated secretion profiles

We first carried out studies based on simulated sensor signals to test the ability of our root-finding algorithm to identify secretion rates. The geometry and dimensions used in simulations are shown in Fig. 5(a). Cells were assumed to be captured in a ring-shaped region (gray area) with electrode located in the middle (gold circle). A secretion pattern was prescribed and the sensor signals were obtained using COMSOL model. The sensor signals were entered into our MATLAB script to calculate the secretion rate without any information of the prescribed secretion pattern. The MATLAB script gave us a series of calculated secretion rates. By comparing calculated secretion rates to the prescribed ones, we found that the root-finding algorithm could successfully retrieve the prescribed secretion rates even the secretion pattern was complicated.

Figures 5(b) and 5(c) show simulated sensor signal and secretion rates based on the input of constant secretion rate. Figs. 5(d) and 5(e) show the simulated signals and the calculated secretion rate based on in the input of exponentially increasing secretion rate. Comparison of Figs. 5(b) and 5(d) shows that the secretion rate from cells in this sensing configuration has a relationship to the gradient of the signal. A large slope in signals indicates a higher secretion rate (when the sensor is far away from saturation). There are two signal jumps at 60 min and

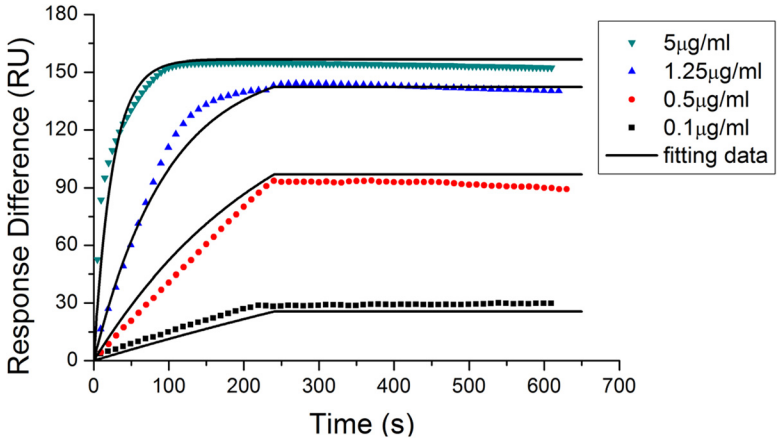

FIG. 4. SPR analysis of IFN-γ aptamer binding kinetics.

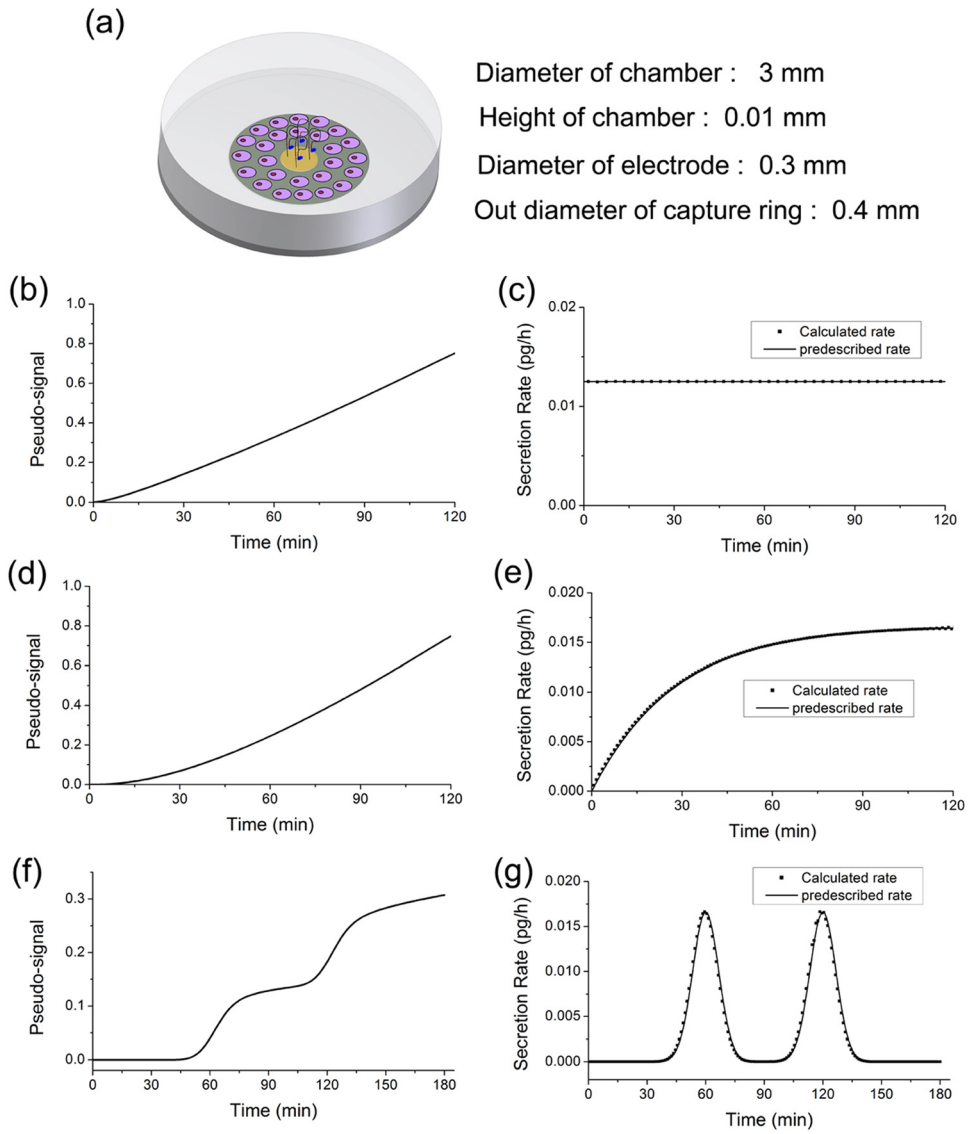

FIG. 5. Results of numerical verification. (a) Geometry and dimension used in simulations. (b) and (c) Signals and calculated rate based on a constant secretion rate. (d) and (e) Signals and calculated rate based on an exponentially increasing secretion rate. (f) and (g) Signals and calculated rate based on two pulse secretion rates.

120 min in Fig. 5(f), indicating two secretion pulses. However, the derivative of the sensor signal cannot be simply used to determine the secretion rate. While the secretion rate is the release rate of molecule from the cell capture region, the derivative of signal reflects the influx of molecules to the sensor. Their relationship is not always linear and affected by other factors such as the existing molecules in the environment. An example was shown in Figs. 5(f) and 5(g). While the cells stop secretion after 150 min, the signal still increased because of existing molecules in the domain.

C. Using microfluidic device with integrated aptasensors to experimentally test model validity

In order to experimentally verify validity of the algorithm for determining secretion rates, we set up a series of experiments using reconfigurable microfluidic devices with integrated aptasensors for IFN-γ detection.[34] These devices, described diagrammatically in

Figs. 1(b), 1(c), and 2, allowed to place a small group of T cells in the proximity of a miniature IFN-γ aptasensor and to detect release of this cytokine. The devices could be reconfigured, with microstructured roof descending onto the cells, stopping diffusion of IFN-γ and isolating cells from the rest of the microfluidic device (Fig. 2). The actuation of the device was used to chemically regenerate the sensor without affecting (lysing) nearby cells. Thus the device could operate in two modes: (1) continuous detection of cell-secreted IFN-γ and (2) discontinuous detection of cell-secreted signal with a series of sense-regenerate cycles.

Figure 6(a) shows a bright-field image of CD4 T cells residing inside the microcups next to a 300 μm diameter sensing electrode. Continuous measurements were taken every 10 min for 2.5 h post stimulation. A typical binding curve resulting from detection of T-cell-secreted IFN-γ

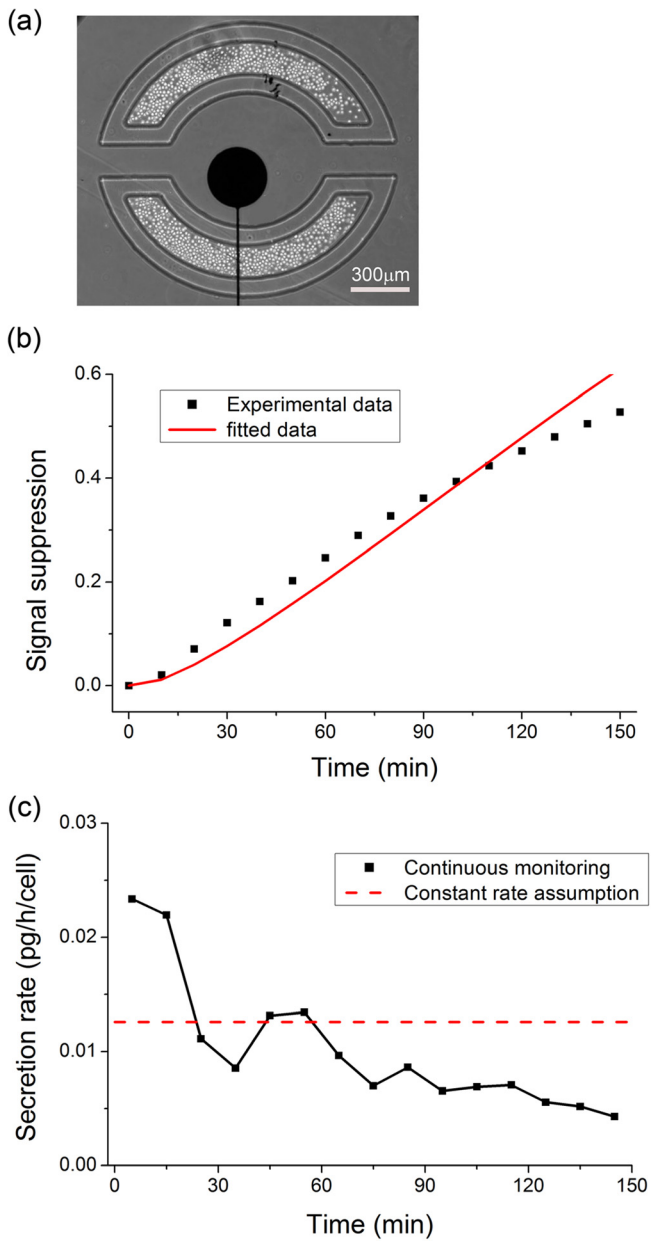

FIG. 6. Signal suppression in continuous detection and calculated secretion rates. (a) A bright-field image of CD4 T cells captured inside PDMS microcups. (b) Signal suppression from a continuous monitoring of 2.5 h. (c) Calculated dynamic secretion rates based on the signal suppressions (-■-) and a constant rate (- - -).

is shown in Fig. 6(b). In the previous studies, our approach was to assume a constant secretion rate and then determine this secretion rate by feeding prediction rates into reaction-diffusion model and looking for best fit to experimental data through least squares approximation. Red line in Fig. 6(b) shows how prediction of single secretion rate ($\dot{\sigma} = 0.012\text{pg/h/cell}$) fits with experimental data. While the fit is satisfactory, single rate prediction underestimates early signals and overestimates late signals.

Applying newly developed algorithm, we obtained multiple secretion rates based on the binding curve shown in Fig. 6(b). In the results presented in Fig. 6(c), the secretion rate was assumed to be constant over a 10 min time interval so that a new rate was calculated for each new time interval. As seen from these data, the production of IFN-γ was high initially (0.023 pg/h/cell) and decreased over time (0.0045 pg/h/cell at last time points).

To prove validity of dynamic rate determination presented in Fig. 6(c), we set up an experiment leveraging discontinuous operation mode of the microfluidic device. The algorithm works by determining secretion rates at small time intervals. To mimic this, we employed the reconfigurable microfluidic device to break up cell secretion experiment lasting 120 min into four time intervals. Fig. 2 describes steps involved in operating the microfluidic device to detect

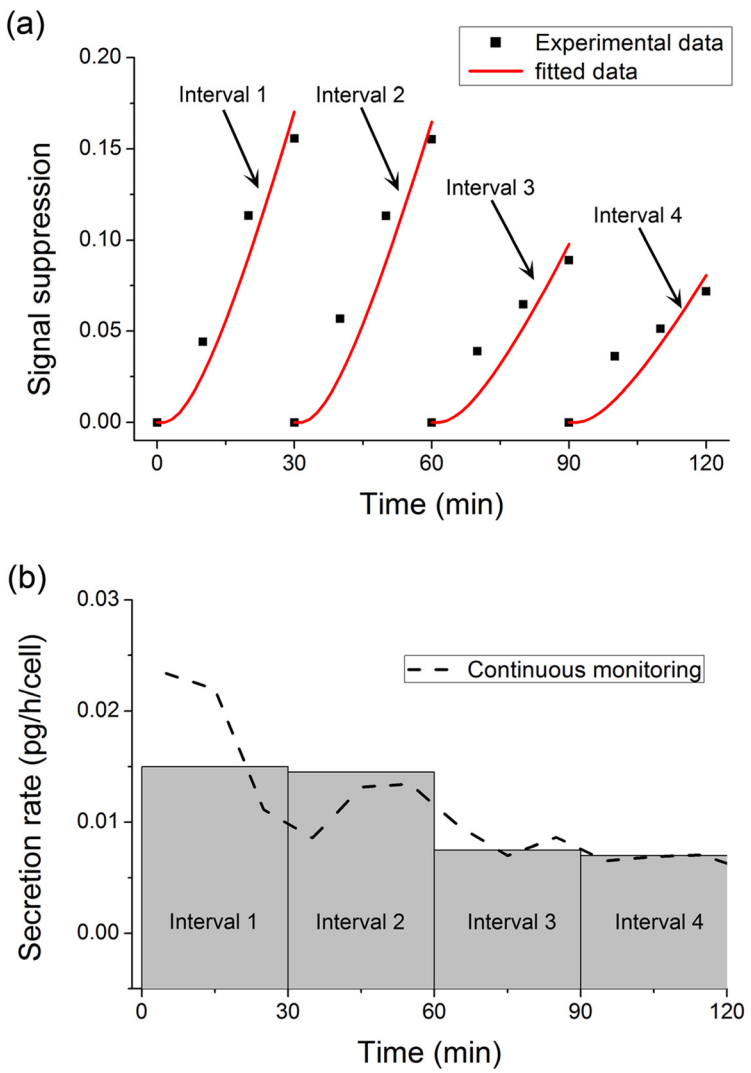

FIG. 7. Signal suppressions in phased detection and calculated secretion rates. (a) Signal suppressions from a phased monitoring of 2 h. (b) Secretion rates in each cycle (calculated dynamic secretion rates from continuous monitoring from Fig. 6 were also added for comparison).

TABLE II. Secretion rate at each time interval.

Time interval (30 min)	Secretion rate (pg/h/cell)
1	0.0151
2	0.0145
3	0.0075
4	0.0070

the signal, regenerate the sensor, and then detect again. Secreted IFN-γ was allowed to accumulate on the sensor surface for 30 min (signal going up in time interval 1), the device was then reconfigured to protect cells inside the microcups and the sensor was regenerated by infusion of urea buffer. The device was reconfigured once again to raise the microcups and recommence signal accumulation for another 30 min time interval. As shown in Fig. 7(a), the cycle of signal collection and sensor regeneration was repeated four times. In our previous study, we verified that the reconfigurable device effectively protected cells from the harsh regeneration buffer.[34] We also determined that regeneration efficiency of the sensor surface was nearly 100% for up to eight cycles. Thus, the decrease in IFN-γ production from first to fourth time interval should be attributed to lower cell secretion rates. The secretion rates in each time interval were determined by the single-rate method using least squares approximation. The resultant rates are compiled in Table II.

Plotting the secretion rates from Table II alongside the secretion rates extracted mathematically from a single continuous secretion experiment revealed a similar downward trend in the IFN-γ production (Fig. 7(b)). This provides experimental prove that a mathematical algorithm may be used to determine up and down changes in secretion rates.

One may ask, why develop more involved mathematical methods for rate determination if it is possible to deploy a reconfigurable device and measure the rates experimentally? The mathematical method may provide hundreds or thousands of values over the course of a secretion experiment and obviates the need for frequent actuation of the microfluidic device. In fact, we envision utilizing mathematical model until the sensor reaches saturation at which point reconfigurable device may be used to regenerate the sensor. This may allow us to both quantify cell secretion and extend the time of sensor operation. Furthermore, a similar mathematical algorithm would work in detection experiments and geometries where microfluidic device of this type may not practical.

V. CONCLUSIONS

Given the increasing emphasis on dynamic monitoring of cell activity, we wanted to develop a mathematical framework for determining dynamic cell secretion rates. This framework was comprised of FEM modeling of diffusion-reaction processes coupled to root-finding algorithm. A microsystem with integrated aptasensor for detecting IFN-γ release from T cells was employed to experimentally prove validity of the mathematical model. This microsystem was designed to operate in two signal collection modes: (1) continuous where IFN-γ released from cells was allowed to accumulate on the sensor surface and (2) discontinuous where signal accumulation was broken down into 4 time intervals. By applying a mathematical algorithm to the continuous detection mode, we were able to extract multiple secretion rates and demonstrate a downward trend in secretion rate over time. By deploying a microfluidic device in a discontinuous operating mode, we determined secretion rates for several time intervals and demonstrated a similar downward trend in the rate of IFN-γ release over time, suggesting decrease in cellular production of IFN-γ after stimulation. These experiments point to the validity of the newly developed mathematical framework for deriving cell secretion rates from biosensor binding curves. Importantly, the mathematical framework described here is general and, after

accounting for the specific geometry and reaction conditions, may be applied to any biosensor continuously measuring molecules being released from cells.

ACKNOWLEDGMENTS

Financial support for this project was provided by NSF Grant Nos. 0937997 and 1160262. Timothy Kwa was supported by NIH fellowship No. T32NIBIB 5T32EB003827. Additional funding came from "Research Investments in Science and Engineering from UC Davis."

[1]A. G. Frutos and R. M. Corn, Anal. Chem. **70**, 449a (1998).
[2]J. Janata, M. Josowicz, P. Vanysek, and D. M. DeVaney, Anal. Chem. **70**, 179 (1998).
[3]A. J. Qavi, A. L. Washburn, J. Y. Byeon, and R. C. Bailey, Anal. Bioanal. Chem. **394**, 121 (2009).
[4]W. H. Tan, K. M. Wang, and T. J. Drake, Curr. Opin. Chem. Biol. **8**, 547 (2004).
[5]J. W. J. Li, X. H. Fang, and W. H. Tan, Biochemi. Biophys. Res. Commun. **292**, 31 (2002).
[6]T. G. McCauley, N. Hamaguchi, and M. Stanton, Anal. Biochem. **319**, 244 (2003).
[7]N. Hamaguchi, A. Ellington, and M. Stanton, Anal. Biochem. **294**, 126 (2001).
[8]A. E. Radi, J. L. A. Sanchez, E. Baldrich, and C. K. O'Sullivan, J. Am. Chem. Soc. **128**, 117 (2006).
[9]R. Y. Lai, K. W. Plaxco, and A. J. Heeger, Anal. Chem. **79**, 229 (2007).
[10]A. A. Lubin and K. W. Plaxco, Acc. Chem. Res. **43**, 496 (2010).
[11]Y. Xiao, A. A. Lubin, A. J. Heeger, and K. W. Plaxco, Angew. Chem., Int. Ed. **44**, 5456 (2005).
[12]Y. Liu, N. Tuleouva, E. Ramanculov, and A. Revzin, Anal. Chem. **82**, 8131 (2010).
[13]N. Tuleuova, C. N. Jones, J. Yan, E. Ramanculov, Y. Yokobayashi, and A. Revzin, Anal. Chem. **82**, 1851 (2010).
[14]J. Kirsch, C. Siltanen, Q. Zhou, A. Revzin, and A. Simonian, Chem. Soc. Rev. **42**, 8733 (2013).
[15]A. Revzin, E. Maverakis, and H. C. Chang, Biomicrofluidics **6**, 21301 (2012).
[16]U. Boehm, T. Klamp, M. Groot, and J. C. Howard, Annu. Rev. Immunol. **15**, 749 (1997).
[17]G. Pantaleo and R. A. Koup, Nat. Med. **10**, 806 (2004).
[18]S. Romagnani, Clin. Immunol. Immunopathol. **80**, 225 (1996).
[19]J. C. Love, J. L. Ronan, G. M. Grotenbreg, A. G. van der Veen, and H. L. Ploegh, Nat. Biotechnol. **24**, 703 (2006).
[20]A. O. Ogunniyi, C. M. Story, E. Papa, E. Guillen, and J. C. Love, Nat. Protoc. **4**, 767 (2009).
[21]Y. J. Yamanaka, C. T. Berger, M. Sips, P. C. Cheney, G. Alter, and J. C. Love, Integr. Biol. (Cambridge) **4**, 1175 (2012).
[22]A. L. Washburn, L. C. Gunn, and R. C. Bailey, Anal. Chem. **81**, 9499 (2009).
[23]A. L. Washburn and R. C. Bailey, Analyst **136**, 227 (2011).
[24]J. T. Kindt and R. C. Bailey, Curr Opin Chem Biol **17**, 818 (2013).
[25]M. G. Roper, J. G. Shackman, G. M. Dahlgren, and R. T. Kennedy, Anal. Chem. **75**, 4711 (2003).
[26]Y. S. Torisawa, N. Ohara, K. Nagamine, S. Kasai, T. Yasukawa, H. Shiku, and T. Matsue, Anal. Chem. **78**, 7625 (2006).
[27]A. M. Clark, K. M. Sousa, C. Jennings, O. A. MacDougald, and R. T. Kennedy, Anal. Chem. **81**, 2350 (2009).
[28]J. G. Shackman, G. M. Dahlgren, J. L. Peters, and R. T. Kennedy, Lab Chip **5**, 56 (2005).
[29]R. Davidsson, B. Johansson, V. Passoth, M. Bengtsson, T. Laurell, and J. Emneus, Lab Chip **4**, 488 (2004).
[30]G. Stybayeva, M. Kairova, E. Ramanculov, A. L. Simonian, and A. Revzin, Colloids Surf. B: Biointerfaces **80**, 251 (2010).
[31]M. W. Li, D. M. Spence, and R. S. Martin, Electroanalysis **17**, 1171 (2005).
[32]Y. Liu, T. Kwa, and A. Revzin, Biomaterials **33**, 7347 (2012).
[33]Y. Liu, J. Yan, M. C. Howland, T. Kwa, and A. Revzin, Anal. Chem. **83**, 8286 (2011).
[34]Q. Zhou, T. Kwa, Y. Gao, Y. Liu, A. Rahimian, and A. Revzin, Lab Chip **14**, 276 (2014).
[35]J. C. McDonald and G. M. Whitesides, Acc. Chem. Res. **35**, 491 (2002).
[36]Y. N. Xia and G. M. Whitesides, Annu. Rev. Mater. Sci. **28**, 153 (1998).
[37]Y. D. Gao, D. Majumdar, B. Jovanovic, C. Shaifer, P. C. Lin, A. Zijlstra, D. J. Webb, and D. Y. Li, Biomed. Microdevices **13**, 539 (2011).
[38]D. Majumdar, Y. D. Gao, D. Y. Li, and D. J. Webb, J. Neurosci. Methods **196**, 38 (2011).
[39]H. Bang, W. G. Lee, J. Park, H. Yun, J. Lee, S. Chung, K. Cho, C. Chung, D. C. Han, and J. K. Chang, J. Micromech. Microeng. **16**, 708 (2006).
[40]M. T. Tyn and T. W. Gusek, Biotechnol. Bioeng. **35**, 327 (1990).
[41]R. J. White, N. Phares, A. A. Lubin, Y. Xiao, and K. W. Plaxco, Langmuir **24**, 10513 (2008).
[42]T. M. Squires, R. J. Messinger, and S. R. Manalis, Nat. Biotechnol. **26**, 417 (2008).
[43]R. A. Vijayendran, F. S. Ligler, and D. E. Leckband, Anal. Chem. **71**, 5405 (1999).
[44]See supplementary material at http://dx.doi.org/10.1063/1.4874216 for more information.
[45]R. P. Brent, *Algorithms for Minimization Without Derivatives* (Prentice-Hall, Englewood Cliffs, NJ, 1972).
[46]W. H. Press, *Numerical Recipes in FORTRAN: The Art of Scientific Computing*, 2nd ed. (Cambridge University Press, Cambridge, England; New York, NY, USA, 1992).